Optimization using Finite Element Models

Dehaeze Thomas

February 26, 2025

Contents

- In the detail design phase, one goal is to optimize the design of the nano-hexapod
- Parts are usually optimized using Finite Element Models that are used to estimate the static and dynamical properties of parts
- However, it is important to see how to dynamics of each part combines with the nano-hexapod and with the micro-station. One option would be to use a FEM of the complete NASS, but that would be very complex and it would be difficult to perform simulations of experiments with real time control implemented.
- The idea is therefore to combine FEM with the multi body model of the NASS. To do so, Reduced Order Flexible Bodies are used (Section 1)
  - The theory is described
  - The method is validated using experimental measurements
- Two main elements of the nano-hexapod are then optimized:
  - The actuator (Section 2)
  - The flexible joints (Section 3)

1 Reduced order flexible bodies

Components exhibiting complex dynamical behavior are frequently found to be unsuitable for direct implementation within multi-body models. These components are traditionally analyzed using Finite Element Analysis (FEA) software. However, a methodological bridge between these two analytical approaches has been established, whereby components whose dynamical properties have been determined through FEA can be successfully integrated into multi-body models [1]. This combined multibody-FEA modeling approach presents significant advantages, as it enables the selective application of FEA modeling to specific elements while maintaining the computational efficiency of multi-body analysis for the broader system [2].

The investigation of this hybrid modeling approach is structured in three sections. First, the fundamental principles and methodological approaches of this modeling framework are introduced (Section 1.1). It is then illustrated through its practical application to the modelling of an Amplified Piezoelectric Actuator (APA) (Section 1.2). Finally, the validity of this modeling approach is demonstrated through experimental validation, wherein the obtained dynamics from the hybrid modelling approach is compared with measurements (Section 1.3).

1.1 Procedure

In this modeling approach, some components within the multi-body framework are represented as *reduced-order flexible bodies*, wherein their modal behavior is characterized through reduced mass and stiffness matrices derived from finite element analysis (FEA) models. These matrices are generated via modal reduction techniques, specifically through the application of component mode synthesis (CMS), thus establishing this design approach as a combined multibody-FEA methodology.

Standard FEA implementations typically involve thousands or even hundreds of thousands of DoF, rendering direct integration into multi-body simulations computationally prohibitive. The objective of modal reduction is therefore to substantially decrease the number of DoF while preserving the essential dynamic characteristics of the component.

The procedure for implementing this reduction involves several distinct stages. Initially, the component is modeled in a finite element software with appropriate material properties and boundary conditions. Subsequently, interface frames are defined at locations where the multi-body model will establish connections with the component. These frames serve multiple functions, including connecting to other parts, applying forces and torques, and measuring relative motion between defined frames.

Following the establishment of these interface parameters, modal reduction is performed using the Craig-Bampton method [3] (also known as the "fixed-interface method"), a technique that transforms the extensive FEA degrees of freedom into a significantly reduced set of retained degrees of freedom. This transformation typically reduces the model complexity from hundreds of thousands to fewer than 100 DoF. The number of degrees of freedom in the reduced model is determined by (1.1) where n represents the number of defined frames and p denotes the number of additional modes to be modeled. The outcome

of this procedure is an $m \times m$ set of reduced mass and stiffness matrices, which can subsequently be incorporated into the multi-body model to represent the component's dynamic behavior.

$$m = 6 \times n + p \tag{1.1}$$

1.2 Example with an Amplified Piezoelectric Actuator

The presented modeling framework was first applied to an Amplified Piezoelectric Actuator (APA) for several reasons. Primarily, this actuator represents an excellent candidate for implementation within the nano-hexapod, as will be elaborated in Section 2. Additionally, an Amplified Piezoelectric Actuator (the APA95ML shown in Figure 1.1) was available in the laboratory for experimental testing.

The APA consists of multiple piezoelectric stacks arranged horizontally (depicted in blue in Figure 1.1) and of an amplifying shell structure (shown in red) that serves two purposes: the application of pre-stress to the piezoelectric elements and the amplification of their displacement into the vertical direction [4]. The selection of the APA for validation purposes was further justified by its capacity to simultaneously demonstrate multiple aspects of the modeling framework. The specific design of the APA allows for the simultaneous modeling of a mechanical structure analogous to a flexible joint, piezoelectric actuation, and piezoelectric sensing, thereby encompassing the principal elements requiring validation.

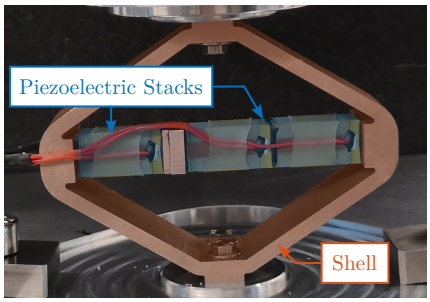

Figure 1.1: Picture of the APA95ML

Parameter	Value
Nominal Stroke	$100\,\mu m$
Blocked force	$2100\,N$
Stiffness	$21\,N/\mu m$

Table 1.1: APA95ML specifications

Finite Element Model The development of the finite element model for the APA95ML necessitated the specification of appropriate material properties, as summarized in Table 1.2. The finite element mesh, shown in Figure 1.2a, was then generated.

Table 1.2: Material properties used for FEA modal reduction model. E is the Young's modulus, ν the Poisson ratio and ρ the material density

	E	ν	ρ
Stainless Steel	$190\,GPa$	0.31	$7800\,\mathrm{kg}/m^3$
Piezoelectric Ceramics (PZT)	$49.5\,GPa$	0.31	$7800\,\mathrm{kg}/m^3$

The definition of interface frames, or "remote points", constitute a critical aspect of the model preparation. Seven frames were established: one frame at the two ends of each piezoelectric stack to facilitate strain measurement and force application, and additional frames at the top and bottom of the structure to enable connection with external elements in the multi-body simulation.

Six additional modes were considered, resulting in total model order of 48. The modal reduction procedure was then executed, yielding the reduced mass and stiffness matrices that form the foundation of the component's representation in the multi-body simulation environment.

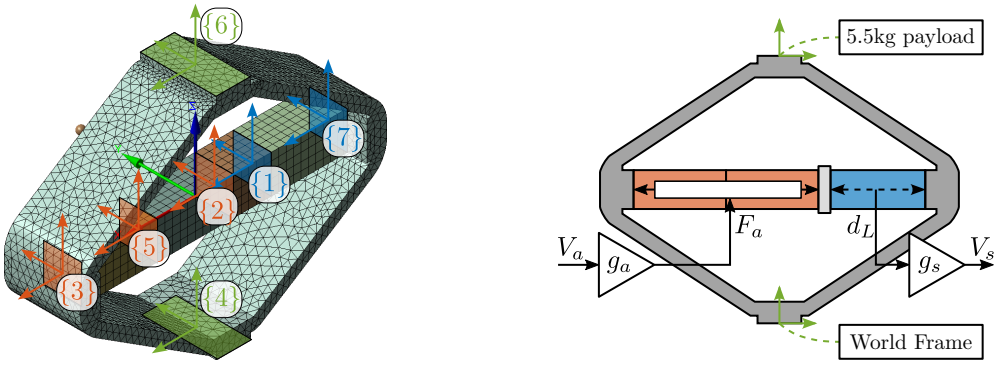

(a) Obtained mesh and "remote points" **(b)** Inclusion in multi-body model

Figure 1.2: Obtained mesh and defined interface frames (or "remote points") in the finite element model of the APA95ML (a). Interface with the multi-body model is shown in (**??**).

Super Element in the Multi-Body Model Previously computed reduced order mass and stiffness matrices were imported in a multi-body model block called "Reduced Order Flexible Solid". This block has several interface frames corresponding to the ones defined in the FEA software. Frame {4} was connected to the "world" frame, while frame {6} was coupled to a vertically guided payload. In this example, two piezoelectric stacks were used for actuation while one piezoelectric stack was used as a force sensor. Therefore, a force source F_a operating between frames {3} and {2} was used, while a displacement sensor d_L between frames {1} and {7} was used for the sensor stack. This is illustrated in Figure 1.2b.

However, to have access to the physical voltage input of the actuators stacks V_a and to the generated voltage by the force sensor V_s, conversion between the electrical and mechanical domains need to be determined.

Sensor and Actuator "constants" To link the electrical domain to the mechanical domain, an "actuator constant" g_a and a "sensor constant" g_s were introduced as shown in Figure 1.2b.

From [5, p. 123], the relation between relative displacement d_L of the sensor stack and generated voltage V_s is given by (1.2).

$$V_s = g_s \cdot d_L, \quad g_s = \frac{d_{33}}{\epsilon^T s^D n} \tag{1.2}$$

From [6] the relation between the force F_a and the applied voltage V_a is given by (1.3).

$$F_a = g_a \cdot V_a, \quad g_a = d_{33} n k_a, \quad k_a = \frac{c^E A}{L} \tag{1.3}$$

Unfortunately, it is difficult to know exactly which material is used in the amplified piezoelectric actuator[1]. However, based on the available properties of the stacks in the data-sheet (summarized in Table 1.3), the soft Lead Zirconate Titanate "THP5H" from Thorlabs seemed to match quite well the observed properties.

Table 1.3: Stack Parameters

Parameter	Unit	Value
Nominal Stroke	μm	20
Blocked force	N	4700
Stiffness	$N/\mu m$	235
Voltage Range	V	-20 to 150
Capacitance	μF	4.4
Length	mm	20
Stack Area	mm^2	10x10

The properties of this "THP5H" material used to compute g_a and g_s are listed in Table 1.4. From these parameters, $g_s = 5.1\,V/\mu m$ and $g_a = 26\,N/V$ were obtained.

Table 1.4: Piezoelectric properties used for the estimation of the sensor and actuators sensitivities

Parameter	**Value**	**Description**
d_{33}	$680 \cdot 10^{-12}\,m/V$	Piezoelectric constant
ϵ^T	$4.0 \cdot 10^{-8}\,F/m$	Permittivity under constant stress
s^D	$21 \cdot 10^{-12}\,m^2/N$	Elastic compliance understand constant electric displacement
c^E	$48 \cdot 10^9\,N/m^2$	Young's modulus of elasticity
L	$20\,mm$ per stack	Length of the stack
A	$10^{-4}\,m^2$	Area of the piezoelectric stack
n	160 per stack	Number of layers in the piezoelectric stack

Identification of the APA Characteristics Initial validation of the finite element model and its integration as a reduced-order flexible model within the multi-body model was accomplished through comparative analysis of key actuator characteristics against manufacturer specifications.

The stiffness of the APA95ML was estimated from the multi-body model by computing the axial compliance of the APA95ML (Figure 1.3), which corresponds to the transfer function from a vertical force applied between the two interface frames to the relative vertical displacement between these two frames. The inverse of the DC gain this transfer function corresponds to the axial stiffness of the APA95ML. A value of $23\,N/\mu m$ was found which is close to the specified stiffness in the datasheet of $k = 21\,N/\mu m$.

The multi-body model predicted a resonant frequency under block-free conditions of 2024 Hz (Figure 1.3), which is in agreement with the nominal specification of 2000 Hz.

In order to estimate the stroke of the APA95ML, first the mechanical amplification factor, defined as the ratio between vertical displacement and horizontal stack displacement, needs to be determined. This characteristic was quantified through analysis of the transfer function relating horizontal stack motion to vertical actuator displacement, from which an amplification factor of 1.5 was derived.

[1]The manufacturer of the APA95ML was not willing to share the piezoelectric material properties of the stack.

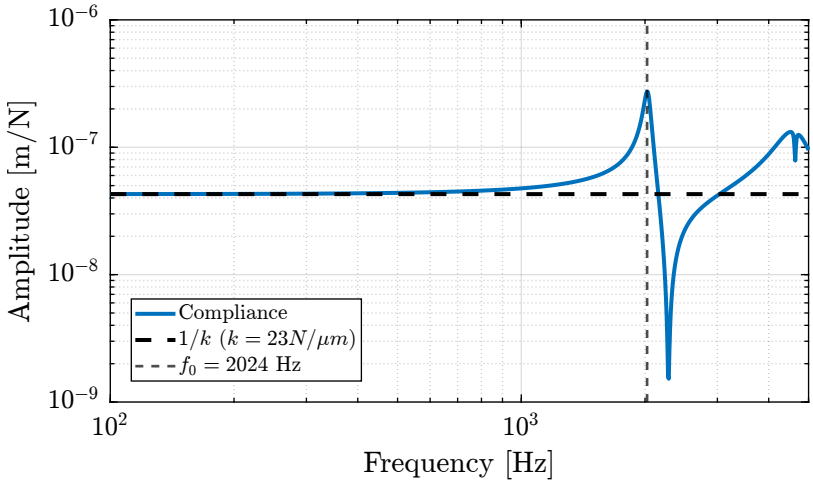

Figure 1.3: Estimated compliance of the APA95ML

The piezoelectric stacks, exhibiting a typical strain response of 0.1 % relative to their length (here equal to $20\,mm$), produce an individual nominal stroke of $20\,\mu m$ (see data-sheet of the piezoelectric stacks on Table 1.3, page 7). As three stacks are used, the horizontal displacement is $60\,\mu m$. Through the established amplification factor of 1.5, this translates to a predicted vertical stroke of $90\,\mu m$ which falls within the manufacturer-specified range of $80\,\mu m$ and $120\,\mu m$.

The high degree of concordance observed across multiple performance metrics provides a first validation of the ability to include FEM into multi-body model.

1.3 Experimental Validation

Further validation of the reduced-order flexible body methodology was undertaken through experimental investigation. The goal is to measure the dynamics of the APA95ML and compared it with predictions derived from the multi-body model incorporating the actuator as a flexible element.

The test bench illustrated in Figure 1.4 was used, which consists of a $5.7\,kg$ granite suspended on top of the APA95ML. The granite's motion was vertically guided with an air bearing system, and a fibered interferometer was used to measured its vertical displacement y. A digital-to-analog converter (DAC) was used to generate the control signal u, which was subsequently conditioned through a voltage amplification stage providing a gain factor of 20, ultimately yielding the effective voltage V_a across the two piezoelectric stacks. Measurement of the sensor stack voltage V_s was performed using an analog-to-digital converter (ADC).

Comparison of the dynamics Frequency domain system identification techniques were used to characterize the dynamic behavior of the APA95ML. The identification procedure necessitated careful choice of the excitation signal **pintelon12˙system˙ident**. The most used ones are impulses (particularly suited to modal analysis), steps, random noise signals, and multi-sine excitations. During all this experimental work, random noise excitation was predominantly employed.

The designed excitation signal is then generated and both input and output signals are synchronously

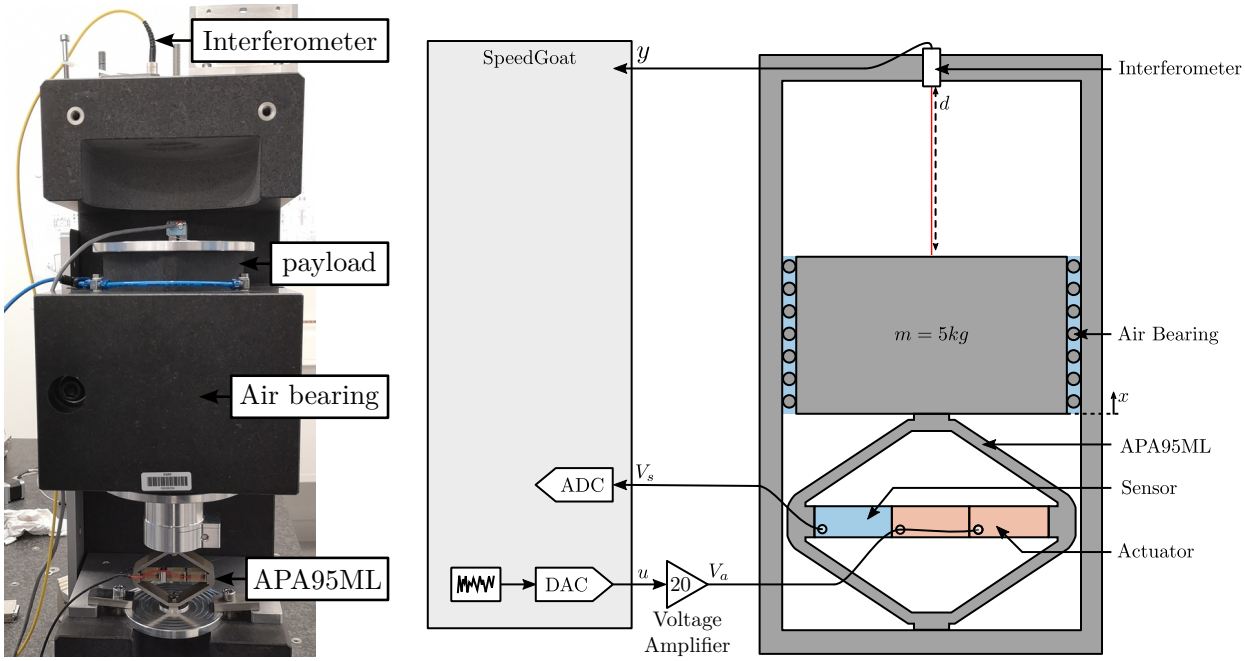

(a) Picture of the test bench

(b) Schematic with signals

Figure 1.4: Test bench used to validate "reduced order solid bodies" using an APA95ML. Picture of the bench is shown in (a). Schematic is shown in (b).

acquired. From the obtained input and output data, the frequency response functions were derived. To improve the quality of the obtained frequency domain data, averaging and windowing were used **pintelon12˙system˙ident**..

The obtained frequency response functions from V_a to V_s and to y are compared with the theoretical predictions derived from the multi-body model in Figure 1.5.

The difference in phase between the model and the measurements can be attributed to the sampling time of $0.1\,ms$ and to additional delays induced by electronic instrumentation related to the interferometer. The presence of a non-minimum phase zero in the measured system response (Figure 1.5b), shall be addressed during the experimental phase.

Regarding the amplitude characteristics, the constants g_a and g_s could be further refined through calibration against the experimental data.

Integral Force Feedback with APA To further validate this modeling methodology, its ability to predict closed-loop behavior was verified experimentally. Integral Force Feedback (IFF) was implemented using the force sensor stack, and the measured dynamics of the damped system were compared with model predictions across multiple feedback gains.

The IFF controller implementation, defined in equation 1.4, incorporated a tunable gain parameter g and was designed to provide integral action near the system resonances and to limit the low frequency gain using an high pass filter.

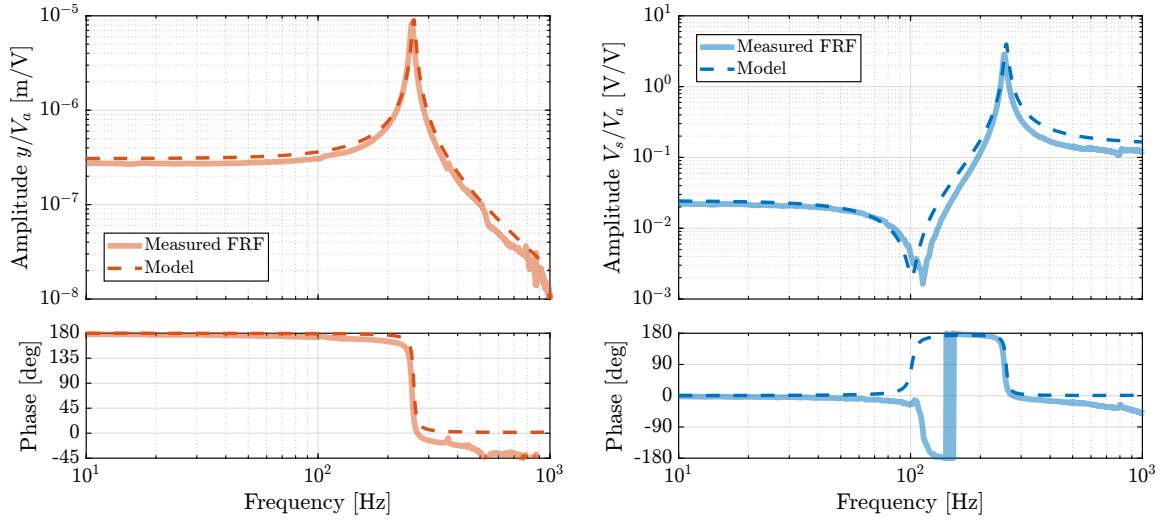

(a) from V_a to y **(b)** from V_a to V_s

Figure 1.5: Comparison of the measured frequency response functions and the identified dynamics from the finite element model of the APA95ML. Both for the dynamics from V_a to y (a) and from V_a to V_s (b)

$$K_{\text{IFF}}(s) = \frac{g}{s + 2 \cdot 2\pi} \cdot \frac{s}{s + 0.5 \cdot 2\pi} \tag{1.4}$$

The theoretical damped dynamics of the closed-loop system was analyzed through using the model by computed the root locus plot shown in Figure 1.6a. For experimental validation, six gain values were tested: $g = [0, 10, 50, 100, 500, 1000]$. The measured frequency responses for each gain configuration were compared with model predictions, as presented in Figure 1.6b.

The close agreement between experimental measurements and theoretical predictions across all gain configurations demonstrates the model's capability to accurately predict both open-loop and closed-loop system dynamics, thereby validating its utility for control system design and analysis.

Conclusion

The modeling procedure presented in this section will demonstrate significant utility for the optimization of complex mechanical components within multi-body systems, particularly in the design of actuators (Section 2) and flexible joints (Section 3).

Through experimental validation using an Amplified Piezoelectric Actuator, the methodology has been shown to accurately predict both open-loop and closed-loop dynamic behavior, thereby establishing its reliability for component design and system analysis.

While this modeling approach provides accurate predictions of component behavior, the resulting model order can become prohibitively high for practical time-domain simulations. This is exemplified by the nano-hexapod configuration, where the implementation of six Amplified Piezoelectric Actuators, each

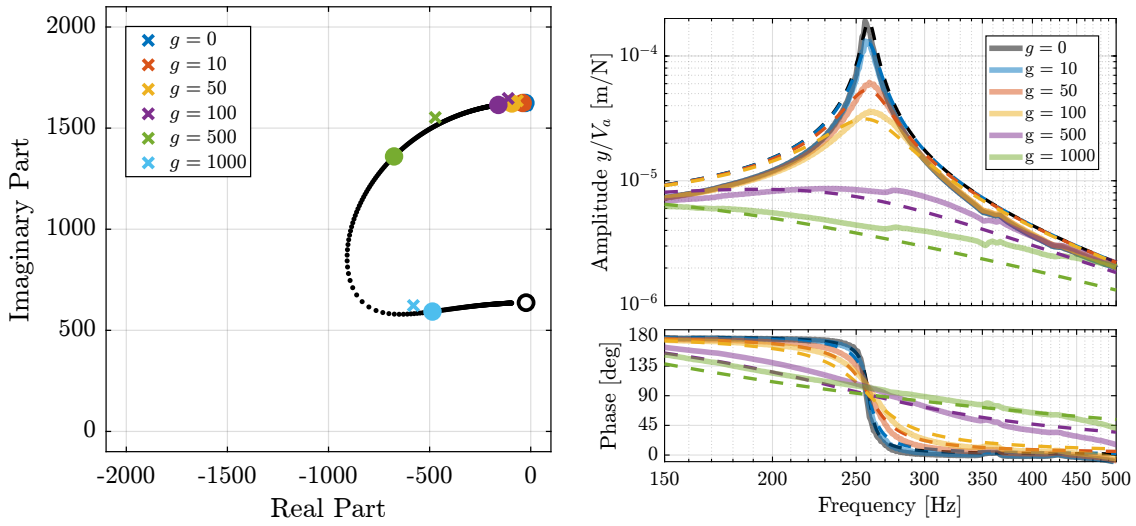

(a) Root Locus plot

(b) Damped plants

Figure 1.6: Obtained results using Integral Force Feedback with the APA95ML. Obtained closed-loop poles as a function of the controller gain g are prediction by root Locus plot (a). Circles are predictions from the model while crosses are poles estimated from the experimental data. Damped plants estimated from the model (dashed curves) and measured ones (solid curves) are compared in (b) for all tested controller gains.

modeled with 48 degrees of freedom, yields 288 degrees of freedom only for the actuators. However, the methodology remains valuable for system analysis, as the extraction of frequency domain characteristics can be efficiently performed even with such high-order models.

2 Actuator Selection

The selection and modeling of actuators constitutes a critical step in the development of the nano-hexapod. This chapter presents the approach to actuator selection and modeling. First, specifications for the nano-hexapod actuators are derived from previous analyses, leading to the selection of the actuator type and ultimately to a specific model (Section 2.1). Then, the chosen actuator is modeled using the reduced-order flexible body approach developed in the previous section, enabling validation of this selection through detailed dynamical analysis (Section 2.2). Finally, a simplified two-degree-of-freedom model is developed to facilitate time-domain simulations while maintaining accurate representation of the actuator's essential characteristics (Section **??**).

2.1 Choice of the Actuator based on Specifications

The actuator selection process was driven by several critical requirements derived from previous dynamic analyses. A primary consideration is the actuator stiffness, which significantly impacts system dynamics through multiple mechanisms. The spindle rotation induces gyroscopic effects that modify plant dynamics and increase coupling, necessitating sufficient stiffness. Conversely, the actuator stiffness must be carefully limited to ensure the nano-hexapod's suspension modes remain below the problematic modes of the micro-stations to limit the coupling between the two structures. These competing requirements suggest an optimal stiffness of approximately $1\,N/\mu m$.

Additional specifications arise from the control strategy and physical constraints. The implementation of a HAC-LAC (High Authority Control-Low Authority Control) architecture necessitates integrated force sensing capability. The system's geometric constraints limit the actuator height to 50mm, given the nano-hexapod's maximum height of 95mm and the presence of flexible joints at each strut extremity. Furthermore, the actuator stroke must exceed the micro-station positioning errors while providing additional margin for mounting adjustments and operational flexibility, which is estimated at $\approx 100\,\mu m$.

Three actuator technologies were evaluated (examples are shown in Figure 2.1): voice coil actuators, piezoelectric stack actuators, and amplified piezoelectric actuators. Variable reluctance actuators were not considered despite their superior efficiency compared to voice coil actuators, as their inherent nonlinearity would introduce unnecessary control complexity.

Voice coil actuators (shown in Figure 2.1a), when combined with flexure guides of wanted stiffness $\approx 1\,N/\mu m$, would require forces above $100\,N$ to achieve the specified $100\,\mu m$ displacement. While these actuators offer excellent linearity and long strokes, the constant force requirement would result in significant steady-state current, leading to thermal loads that could compromise system stability. Their advantages were not considered adapted for this application, diminishing their benefits relative to piezoelectric solutions.

Conventional piezoelectric stack actuators (shown in Figure 2.1b) present two significant limitations for the current application. Their stroke is inherently limited to approximately $0.1\,\%$ of their length, meaning that even with the maximum allowable height of $50\,mm$, the achievable stroke would only be

(a) Voice Coil **(b)** Piezoelectric stack **(c)** Amplified Piezoelectric Actuator

Figure 2.1: Example of actuators considered for the nano-hexapod. Voice coil from Sensata Technologies (a). Piezoelectric stack actuator from Physik Instrumente (b). Amplified Piezoelectric Actuator from DSM (c).

$50\,\mu m$, insufficient for the application. Additionally, their extremely high stiffness, typically around $100\,N/\mu m$, exceeds the desired specifications by two orders of magnitude.

Amplified Piezoelectric Actuators (APAs) emerged as the optimal solution by addressing these limitations through an specific mechanical design. The incorporation of a shell structure serves multiple purposes: it provides mechanical amplification of the piezoelectric displacement, reduces the effective axial stiffness to more suitable levels for the application, and creates a compact vertical profile. Furthermore, the multi-stack configuration enables one stack to be dedicated to force sensing, ensuring excellent collocation with the actuator stacks, a critical feature for implementing robust decentralized control strategies. Moreover, using APA for active damping has been successfully demonstrated in similar applications [7].

Several specific APA models were evaluated against the established specifications (Table 2.1). The APA300ML emerged as the optimal choice. This selection was further reinforced by previous experience with APAs from the same manufacturer[1], and particularly by the successful validation of the modeling methodology with a similar actuator (Section 1.2). The demonstrated accuracy of the modeling approach for the APA95ML provides confidence in the reliable prediction of the APA300ML's dynamic characteristics, thereby supporting both the selection decision and subsequent dynamical analyses.

Table 2.1: List of some amplified piezoelectric actuators that could be used for the nano-hexapod

Specification	APA150M	**APA300ML**	APA400MML	FPA-0500E-P	FPA-0300E-S
Stroke $> 100\,[\mu m]$	187	304	368	432	240
Stiffness $\approx 1\,[N/\mu m]$	0.7	1.8	0.55	0.87	0.58
Resolution $< 2\,[nm]$	2	3	4		
Blocked Force $> 100\,[N]$	127	546	201	376	139
Height $< 50\,[mm]$	22	30	24	27	16

2.2 APA300ML - Reduced Order Flexible Body

The validation of the APA300ML started by incorporating a "reduced order flexible body" into the multi-body model as explained in Section 1. The FEA model was developed with particular attention to

[1] Cedrat technologies

the placement of reference frames, as illustrated in Figure 2.2b. Seven distinct frames were defined, with blue frames designating the force sensor stack interfaces for strain measurement, red frames denoting the actuator stack interfaces for force application and green frames for connecting to other elements. 120 additional modes were added during the modal reduction for a total order of 162. While this high order provides excellent accuracy for validation purposes, it proves computationally intensive for simulations.

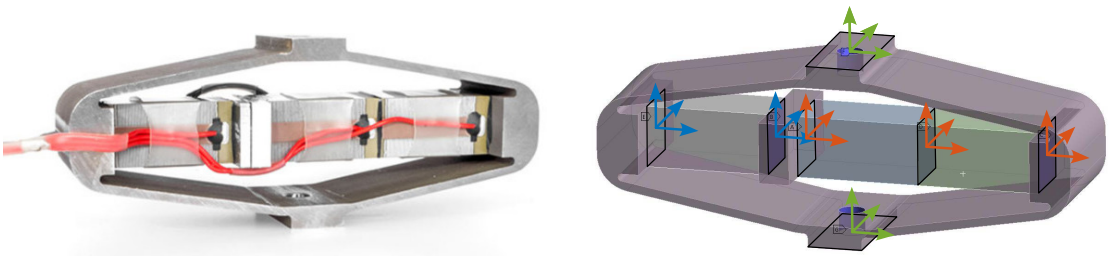

(a) Picture of the APA300ML

(b) FEM of the APA300ML

Figure 2.2: Amplified Piezoelectric Actuator APA300ML. Picture shown in (a). Frames (or "remote points") used for the modal reduction are shown in (b).

The sensor and actuator "constants" (g_s and g_a) derived in Section 1.2 for the APA95ML were used for the APA300ML model, as both actuators employ identical piezoelectric stacks.

2.3 Simpler 2DoF Model of the APA300ML

To facilitate efficient time-domain simulations while maintaining essential dynamic characteristics, a simplified two-degree-of-freedom model was developed, adapted from [8].

This model, illustrated in Figure 2.3, comprises three components. The mechanical shell is characterized by its axial stiffness k_1 and damping c_1. The actuator is modelled with stiffness k_a and damping c_a, incorporating a force source f. This force is related to the applied voltage V_a through the actuator constant g_a. The sensor stack is modeled with stiffness k_e and damping c_e, with its deformation d_L being converted to the output voltage V_s through the sensor sensitivity g_s.

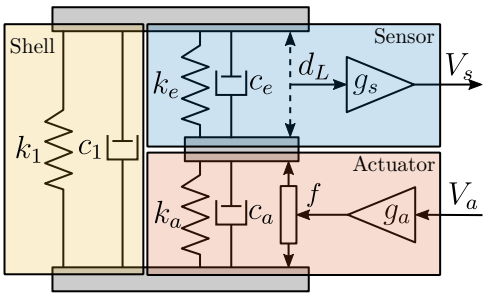

Figure 2.3: Schematic of the 2DoF model of the Amplified Piezoelectric Actuator

While providing computational efficiency, this simplified model has inherent limitations. It considers only axial behavior, treating the actuator as infinitely rigid in other directions. Several physical characteristics are not explicitly represented, including the mechanical amplification factor and the actual

stress the piezoelectric stacks. Nevertheless, the model's primary advantage lies in its simplicity, adding only four states to the system model.

The model requires tuning of 8 parameters (k_1, c_1, k_e, c_e, k_a, c_a, g_s, and g_a) to match the dynamics extracted from the finite element analysis.

The shell parameters k_1 and c_1 were determined first through analysis of the zero in the V_a to V_s transfer function. The physical interpretation of this zero can be understood through Root Locus analysis: as controller gain increases, the poles of a closed-loop system converge to the open-loop zeros. In this context, the zero corresponds to the poles of the system with a theoretical infinite-gain controller that ensures zero force in the sensor stack. This condition effectively represents the dynamics of an APA without the force sensor stack. This physical interpretation enables straightforward parameter tuning: k_1 determines the frequency of the zero, while c_1 defines its damping characteristic.

The stack parameters (k_a, c_a, k_e, c_e) were then derived from the first pole of the V_a to y response. Given that identical piezoelectric stacks are used for both sensing and actuation, the relationships $k_e = 2k_a$ and $c_e = 2c_a$ were enforced, reflecting the series configuration of the dual actuator stacks. Finally, the sensitivities g_s and g_a were adjusted to match the DC gains of the respective transfer functions.

The resulting parameters, documented in Table 2.2, yield dynamic behavior that closely matches the high-order finite element model, as demonstrated in Figure 2.4. While higher-order modes and non-axial flexibility are not captured, the model accurately represents the fundamental dynamics within the operational frequency range.

Table 2.2: Summary of the obtained parameters for the 2 DoF APA300ML model

Parameter	Value
k_1	$0.30\,N/\mu m$
k_e	$4.3\,N/\mu m$
k_a	$2.15\,N/\mu m$
c_1	$18\,Ns/m$
c_e	$0.7\,Ns/m$
c_a	$0.35\,Ns/m$
g_a	$2.7\,N/V$
g_s	$0.53\,V/\mu m$

2.4 Electrical characteristics of the APA

The behavior of piezoelectric actuators is characterized by coupled constitutive equations that establish relationships between electrical properties (charges, voltages) and mechanical properties (stress, strain) **schmidt20˙desig˙high˙perfor˙mechat˙third˙revis˙edition**.

To evaluate the impact of electrical boundary conditions on the system dynamics, experimental measurements were conducted using the APA95ML, comparing the transfer function from V_a to y under two distinct configurations. With the force sensor stack in open-circuit condition (analogous to voltage measurement with high input impedance) and in short-circuit condition (similar to charge measurement with low output impedance). As demonstrated in Figure 2.5, short-circuiting the force sensor stack results in a minor decrease in resonance frequency. This relatively modest effect validates the simplifying assumption made in the model of the APA.

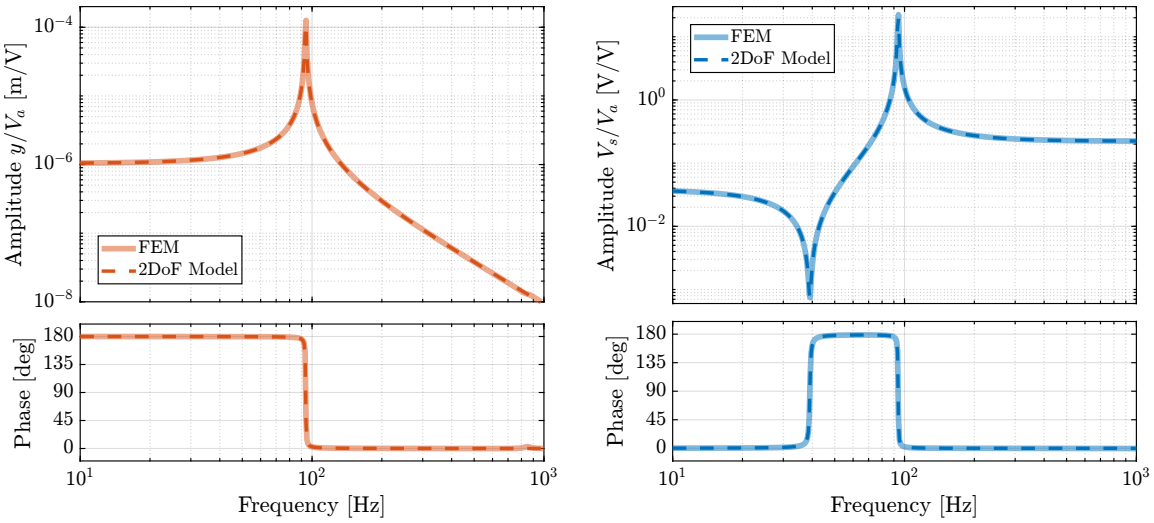

(a) from V_a to d_i **(b)** from V_a to V_s

Figure 2.4: Comparison of the transfer functions extracted from the finite element model of the APA300ML and of the 2DoF model. Both for the dynamics from V_a to d_i (a) and from V_a to V_s (b)

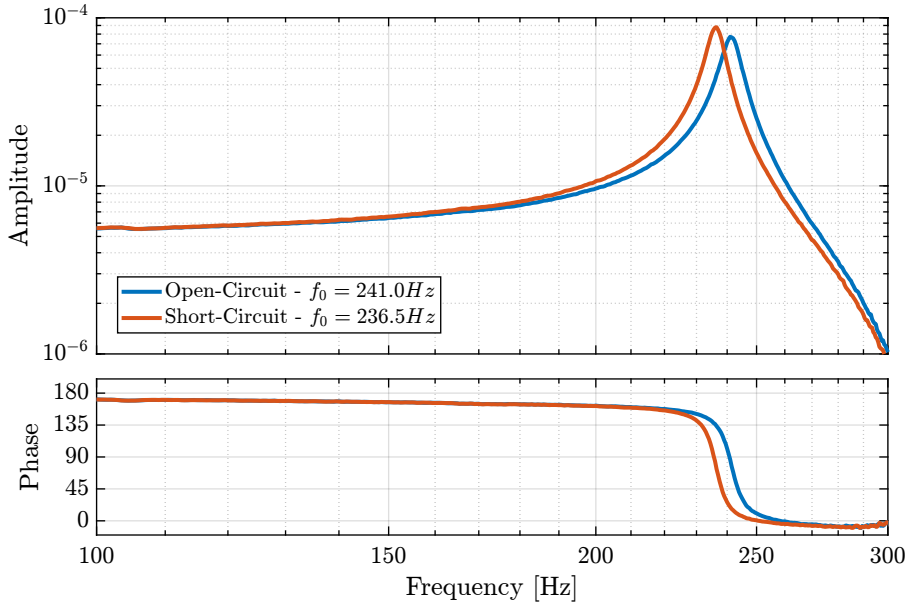

Figure 2.5: Effect of the electrical bondaries of the force sensor stack on the APA95ML resonance frequency

However, the electrical characteristics of the APA remain crucial for instrumentation design. Proper consideration must be given to voltage amplifier specifications and force sensor signal conditioning requirements. These aspects, being fundamental to system implementation, will be addressed in the instrumentation chapter.

2.5 Validation with the Nano-Hexapod

The integration of the APA300ML model within the nano-hexapod simulation framework served two validation objectives: to validate the APA300ML choice through analysis of system dynamics with APA modelled as flexible bodies, and to validate the simplified 2DoF model through comparative analysis with the full FEM implementation.

The dynamic characteristics predicted using the flexible body model align well with the design requirements established during the conceptual phase. The dynamics from $\boldsymbol{u}$ to $\boldsymbol{V}_s$ exhibits the desired alternating pole-zero pattern (Figure 2.6a), a critical characteristic for implementing robust decentralized Integral Force Feedback. Additionally, the model predicts no problematic high-frequency modes in the dynamics from $\boldsymbol{u}$ to $\boldsymbol{\epsilon}_{\mathcal{L}}$ (Figure 2.6b), maintaining consistency with earlier conceptual simulations. These findings suggest that the control performance targets established during the conceptual phase remain achievable with the selected actuator.

Comparative analysis between the high-order FEM implementation and the simplified 2DoF model (Figure 2.6) demonstrates remarkable agreement in the frequency range of interest. This validates the use of the simplified model for time-domain simulations, where computational efficiency is paramount. The reduction in model order is substantial: while the FEM implementation results in approximately 300 states (36 states per actuator plus 12 additional states), the 2DoF model requires only 24 states for the complete nano-hexapod.

These results validate both the selection of the APA300ML and the effectiveness of the simplified modeling approach for the nano-hexapod.

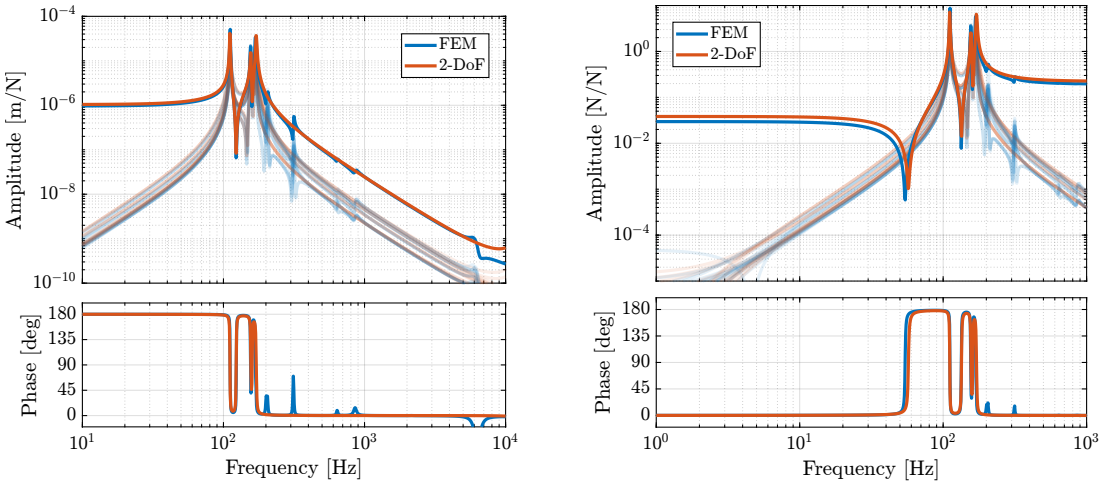

(a) $\boldsymbol{f}$ to $\boldsymbol{\epsilon}_{\mathcal{L}}$ **(b)** $\boldsymbol{f}$ to $\boldsymbol{f}_m$

Figure 2.6: Comparison of the dynamics obtained between a nano-hexpod having the actuators modeled with FEM and a nano-hexapod having actuators modelled a 2DoF system. Both from actuator force $\boldsymbol{f}$ to strut motion measured by external metrology $\boldsymbol{\epsilon}_{\mathcal{L}}$ (b) and to the force sensors $\boldsymbol{f}_m$ (a).

3 Flexible Joint Design

The flexible joints have few advantages compared to conventional joints such as the **absence of wear, friction and backlash** which allows extremely high-precision (predictable) motion. The parasitic bending and torsional stiffness of these joints usually induce some **limitation on the control performance**. [9]

In this document is studied the effect of the mechanical behavior of the flexible joints that are located the extremities of each nano-hexapod's legs.

Ideally, we want the x and y rotations to be free and all the translations to be blocked. However, this is never the case and be have to consider:

- Non-null bending stiffnesses
- Non-null radial compliance
- Axial stiffness in the direction of the legs

This may impose some limitations, also, the goal is to specify the required joints stiffnesses.

Say that for simplicity (reduced number of parts, etc.), we consider the same joints for the fixed based and the top platform.

Outline:

- Perfect flexible joint
- Imperfection of the flexible joint: Model
- Study of the effect of limited stiffness in constrain directions and non-null stiffness in other directions
- Obtained Specification
- Design optimisation (FEM)
- Implementation of flexible elements in the Simscape model: close to simplified model

3.1 Flexible joints for Stewart platforms

Review of different types of flexible joints for Stewart plaftorms (see Figure 3.1).

Typical specifications:

- Bending stroke (i.e. long life time by staying away from yield stress, even at maximum deflection/load)
- Axial stiffness
- Bending stiffness
- Maximum axial load
- Well defined rotational axes

Typical values?

- $K_{\theta,\phi} = 15\,[Nm/rad]$ stiffness in flexion
- $K_{\psi} = 20\,[Nm/rad]$ stiffness in torsion
- $$K_a = 60\,[N/\mu m]$$

  axial stiffness

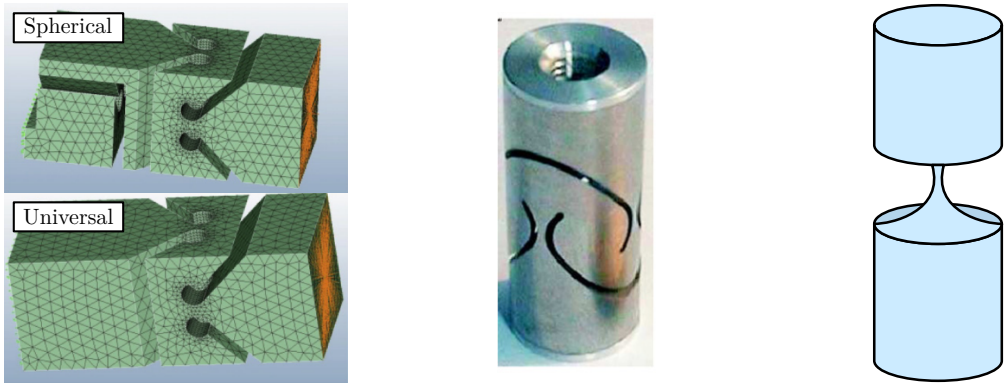

(a) **(b)** **(c)**

Figure 3.1: Example of different flexible joints geometry used for Stewart platforms. (a) [10]. (b) [11]. (c) [12].

3.2 Bending and Torsional Stiffness

Because of bending stiffness of the flexible joints, the forces applied by the struts are no longer aligned with the struts (additional forces applied by the "spring force" of the flexible joints).

In this section, we wish to study the effect of the rotation flexibility of the nano-hexapod joints.

- To simplify the analysis, the micro-station is considered rigid, and only the nano-hexapod is considered with:

  - 1dof actuators, k=1N/um, without parallel stiffness to the force sensors

- The bending stiffness of all joints are varied and the dynamics is identified

HAC plant (transfer function from f to dL, as measured by the external metrology):

- It increase the coupling at low frequency, but is kept to small values for realistic values of the bending stiffness (Figure 3.2a)

- Bending stiffness does not impact significantly the HAC plant. The added stiffness increases the frequency of the suspension modes Condition in [9] to have forces aligned with the struts when considering rotational stiffness: kr ¡¡ k*l^2 For the current nano hexapod configuration, it correspond to ¡¡ 9000 Nm/rad. This may be an issue for soft nano-hexapod (for instance k = 1e4 =¿ ¡¡ 90) =¿ have to design very soft flexible joints. Here, having relatively stiff actuators render this condition easier to achieve.

IFF Plant:

- Having bending stiffness adds complex conjugate zero at low frequency (Figure 3.2b)

- Similar to having a stiffness in parallel to the struts (i.e., to the force sensor). This can be explained since even if the force sensor is removed (i.e. zero axial stiffness of the strut), the strut will still act as a spring between the mobile and fixed plates because of the bending stiffness of the flexible joints. The frequency of the zero gives an idea of the stiffness contribution of the flexible joint bending stiffness

- They therefore impose limitation for decentralized IFF, as discussed in [11]

- This can be seen in the root locus plot of Figure 3.3a

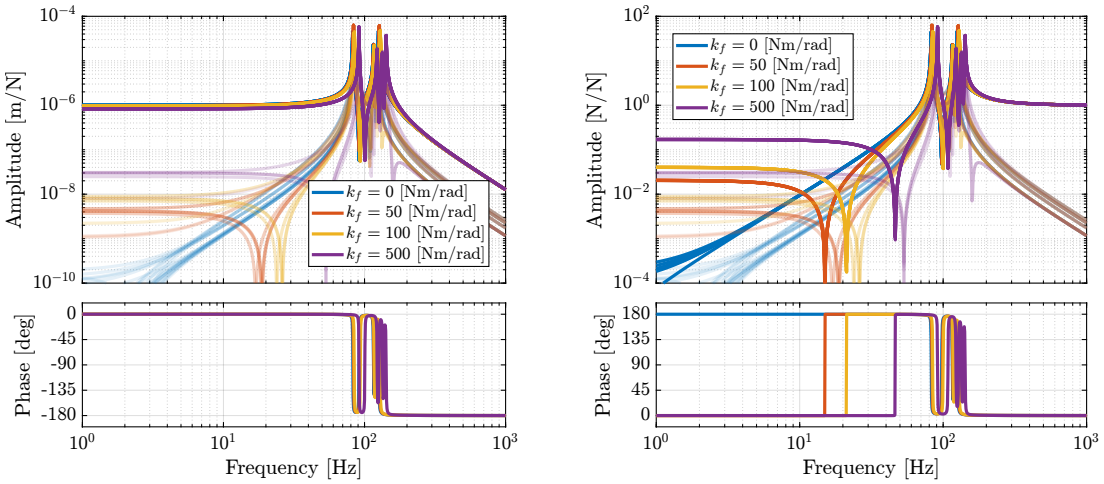

(a) $\boldsymbol{f}$ to $\boldsymbol{\epsilon}_{\mathcal{L}}$ **(b)** $\boldsymbol{f}$ to $\boldsymbol{f}_m$

Figure 3.2: Effect of bending stiffness of the flexible joints on the plant dynamics. Both from actuator force $\boldsymbol{f}$ to strut motion measured by external metrology $\boldsymbol{\epsilon}_{\mathcal{L}}$ (a) and to the force sensors $\boldsymbol{f}_m$ (b)

However, as the APA300ML was chosen for the actuator, stiffness are already present in parallel to the

force sensors:

- The dynamics is computed again for all considered values of the bending stiffnesses with the 2DoF model of the APA300ML
- Root locus for decentralized IFF are shown in Figure 3.3b. Now the effect of bending stiffness has little effect on the attainable damping, as its contribution as "parallel stiffness" is small compared to the parallel stiffness already present in the APA300ML.

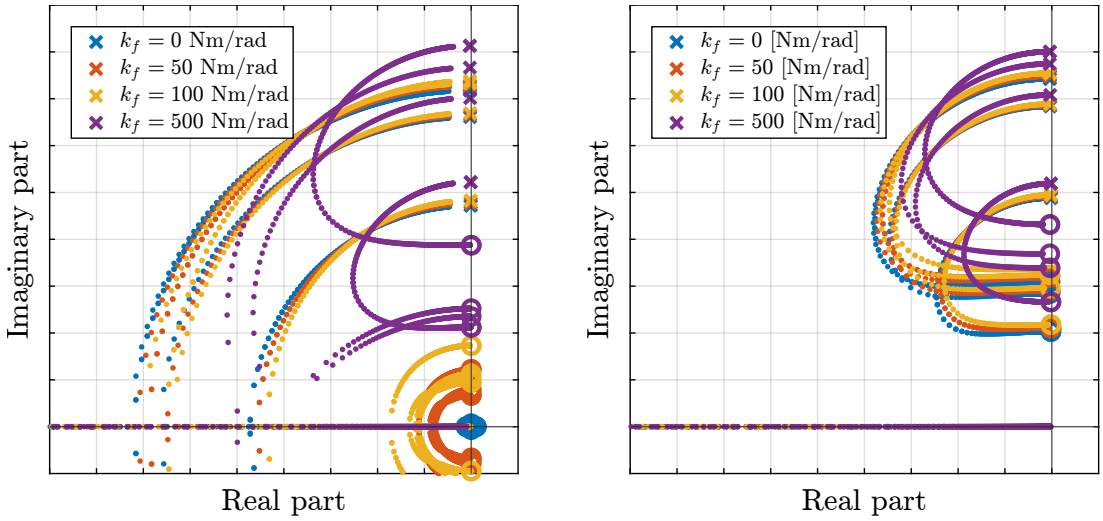

(a) 1DoF actuators **(b)** APA300ML actuators

Figure 3.3: Effect of bending stiffness of the flexible joints on the attainable damping with decentralized IFF. When having an actuator modelled as 1DoF without parallel stiffness to the force sensor (a), and with the 2DoF model of the APA300ML (b)

Conclusion:

- Similar results for torsional stiffness, but less important
- thanks to the use of the APA, the requirements in terms of bending stiffness are less stringent

3.3 Axial Stiffness

- Adding flexibility between the actuation point and the measurement point / point of interest is always detrimental for the control performances. This is verified, and the goal is to estimate the minimum axial stiffness that the flexible joints should have
- Here, the mass of the strut should be considered. It is set to 112g as specified in the APA300ML specification sheet.
- Transfer functions are estimated for several axial stiffnesses (Figure 3.4)
- IFF plant is not much affected (Figure 3.4b). Confirmed by the root locus plot of Figure 3.5a

- "HAC" plant:
  - Additional modes at high frequency corresponding to internal modes of the struts. It adds coupling to the plant. This is confirmed by computed the RGA-number for the damped plant (i.e. after applying decentralized IFF) in Figure 3.5b

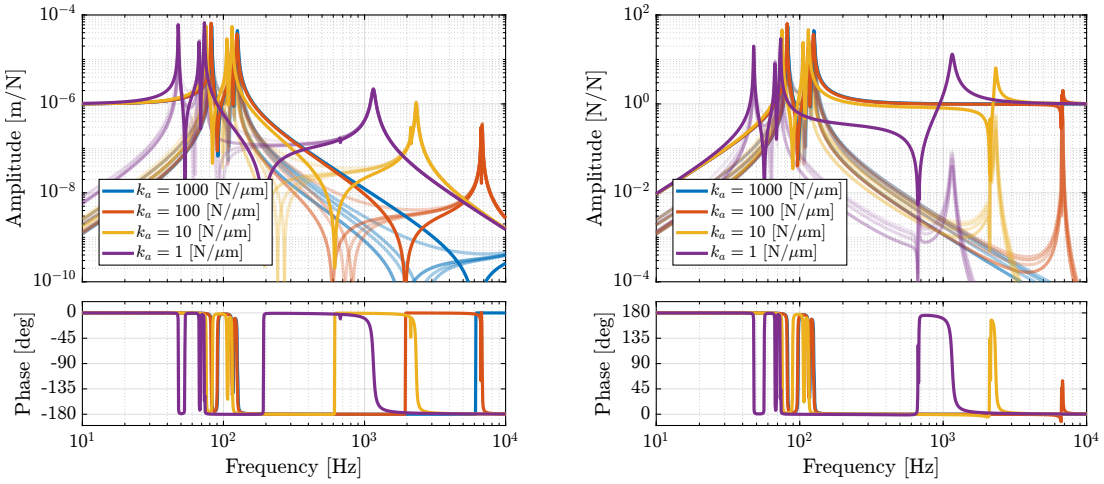

(a) $\boldsymbol{f}$ to $\boldsymbol{\epsilon}_{\mathcal{L}}$ **(b)** $\boldsymbol{f}$ to $\boldsymbol{f}_m$

Figure 3.4: Effect of axial stiffness of the flexible joints on the plant dynamics. Both from actuator force $\boldsymbol{f}$ to strut motion measured by external metrology $\boldsymbol{\epsilon}_{\mathcal{L}}$ (a) and to the force sensors $\boldsymbol{f}_m$ (b)

Integral force feedback

Maybe show the damped plants instead?

Root Locus: not a lot of effect

Conclusion:

- The axial stiffness of the flexible joints should be maximized to limit additional coupling at high frequency that may negatively impact the achievable bandwidth
- It should be much higher than the stiffness of the actuator
- For the nano-hexapod 100N/um is a reasonable axial stiffness specification
- Above the resonance frequency linked to the limited axial stiffness of the flexible joint, the system becomes coupled and impossible to control
- Also, loose control authority at the frequency of the zero

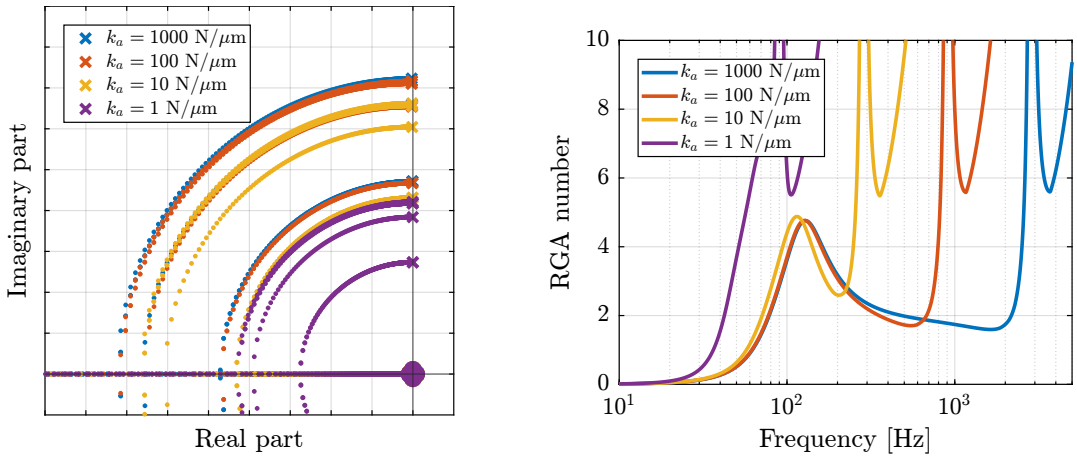

(a) Root Locus

(b) RGA number

Figure 3.5: Effect of axial stiffness of the flexible joints on the attainable damping with decentralized IFF (a). Estimation of the coupling of the damped plants using the RGA-number (b)

3.4 Obtained design / Specifications

- Summary of specifications (Table 3.1)
- Explain choice of geometry:
  - x and y rotations are coincident
  - stiffness can be easily tuned
  - high axial stiffness
- Explain how it is optimized:
  - Extract stiffnesses from FEM
  - Parameterized model in the FE software
  - Quick optimization: (few iterations, could probably increase more the axial stiffness)
    - There is a trade off between high axial stiffness and low bending/torsion stiffness
    - Also check the yield strength
- Show obtained geometry Figure 3.6:
  - "neck" size: 0.25mm
- Characteristics of the flexible joints obtained from FEA are summarized in Table 3.1

Table 3.1: Specifications for the flexible joints and estimated characteristics from the Finite Element Model

	Specification	**FEM**
Axial Stiffness k_a	$> 100\,N/\mu m$	94
Shear Stiffness k_s	$> 1\,N/\mu m$	13
Bending Stiffness k_f	$< 100\,Nm/\text{rad}$	5
Torsion Stiffness k_t	$< 500\,Nm/\text{rad}$	260
Bending Stroke	$> 1\,\text{mrad}$	24.5

(a) 3D view **(b)** Key dimensions

Figure 3.6: Designed flexible joints.

3.5 Validation with the Nano-Hexapod

To validate the designed flexible joint:

- FEM: modal reduction two interface frames are defined (Figure 3.7)
- additional 6 modes are extracted: size of reduced order mass and stiffness matrices: 18×18
- Imported in the multi-body model
- The transfer functions from forces and torques applied between frames $\{F\}$ and $\{M\}$ to the relative displacement/rotations of the two frames is extracted.
- The stiffness characteristics of the flexible joint is estimated from the low frequency gain of the obtained transfer functions. Same values are obtained with the reduced order model and the FEM.

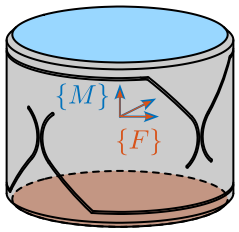

Figure 3.7: Defined frames for the reduced order flexible body. The two flat interfaces are considered rigid, and are linked to the two frames $\{F\}$ and $\{M\}$ both located at the center of the rotation.

Depending on which characteristic of the flexible joint is to be modelled, several DoFs can be taken into account:

- 2DoF (universal joint) k_f
- 3DoF (spherical joint) taking into account torsion k_f, k_t
- 2DoF + axial stiffness k_f, k_a
- 3DoF + axial stiffness k_f, k_t, k_a
- 6DoF ("bushing joint") k_f, k_t, k_a, k_s

Adding more degrees of freedom:

- can represent important features
- adds model states that may not be relevant for the dynamics, and may complexity the simulations without adding much information

After testing different configurations, a good compromise was found for the modelling of the nano-hexapod flexible joints:

- bottom joints: k_f and k_a
- top joints: k_f, k_t and k_a

Talk about model order:

- with flexible joints: 252 states:
  - 12 for the payload (6 dof)
  - 12 for the 2DoF struts
  - 216 DoF for the flexible joints (18*6*2)
  - 12 states for?
- with 3dof and 4dof: 48 states
  - 12 for the payload (6 dof)
  - 12 for the 2DoF struts
  - 12 states for the bottom joints
  - 12 states for the top joints

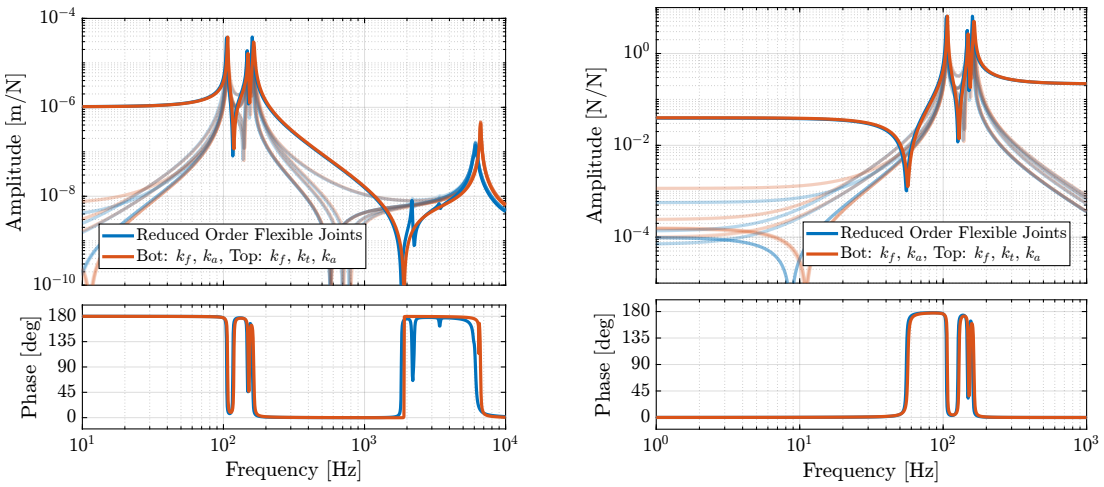

(a) $\boldsymbol{f}$ to $\boldsymbol{\epsilon}_{\mathcal{L}}$ **(b)** $\boldsymbol{f}$ to $\boldsymbol{f}_m$

Figure 3.8: Comparison of the dynamics obtained between a nano-hexpod including joints modelled with FEM and a nano-hexapod having bottom joint modelled by bending stiffness k_f and axial stiffness k_a and top joints modelled by bending stiffness k_f, torsion stiffness k_t and axial stiffness k_a. Both from actuator force $\boldsymbol{f}$ to strut motion measured by external metrology $\boldsymbol{\epsilon}_{\mathcal{L}}$ (b) and to the force sensors $\boldsymbol{f}_m$ (a).

Conclusion

Bibliography

[1] M. R. Hatch, *Vibration simulation using MATLAB and ANSYS*. CRC Press, 2000 (cit. on p. 4).

[2] A. M. Rankers, "Machine dynamics in mechatronic systems: An engineering approach.," Ph.D. dissertation, University of Twente, 1998 (cit. on p. 4).

[3] R. R. CRAIG and M. C. C. BAMPTON, "Coupling of substructures for dynamic analyses.," *AIAA Journal*, vol. 6, no. 7, pp. 1313–1319, 1968 (cit. on p. 4).

[4] F. Claeyssen, R. L. Letty, F. Barillot, and O. Sosnicki, "Amplified piezoelectric actuators: Static & dynamic applications," *Ferroelectrics*, vol. 351, no. 1, pp. 3–14, 2007 (cit. on p. 5).

[5] A. J. Fleming and K. K. Leang, *Design, Modeling and Control of Nanopositioning Systems* (Advances in Industrial Control). Springer International Publishing, 2014 (cit. on p. 6).

[6] A. J. Fleming and K. K. Leang, "Integrated strain and force feedback for high-performance control of piezoelectric actuators," *Sensors and Actuators A: Physical*, vol. 161, no. 1-2, pp. 256–265, 2010 (cit. on p. 6).

[7] A. A. Hanieh, "Active isolation and damping of vibrations via stewart platform," Ph.D. dissertation, Université Libre de Bruxelles, Brussels, Belgium, 2003 (cit. on p. 13).

[8] A. Souleille, T. Lampert, V. Lafarga, *et al.*, "A concept of active mount for space applications," *CEAS Space Journal*, vol. 10, no. 2, pp. 157–165, 2018 (cit. on p. 15).

[9] J. McInroy, "Modeling and design of flexure jointed stewart platforms for control purposes," *IEEE/ASME Transactions on Mechatronics*, vol. 7, no. 1, pp. 95–99, 2002 (cit. on pp. 20, 22).

[10] X. Yang, H. Wu, B. Chen, S. Kang, and S. Cheng, "Dynamic modeling and decoupled control of a flexible stewart platform for vibration isolation," *Journal of Sound and Vibration*, vol. 439, pp. 398–412, Jan. 2019 (cit. on p. 21).

[11] A. Preumont, M. Horodinca, I. Romanescu, *et al.*, "A six-axis single-stage active vibration isolator based on stewart platform," *Journal of Sound and Vibration*, vol. 300, no. 3-5, pp. 644–661, 2007 (cit. on pp. 21, 22).

[12] Z. Du, R. Shi, and W. Dong, "A piezo-actuated high-precision flexible parallel pointing mechanism: Conceptual design, development, and experiments," *IEEE Transactions on Robotics*, vol. 30, no. 1, pp. 131–137, 2014 (cit. on p. 21).